

CHAPTER 5

WIND VELOCITY PROFILE ABOVE PROGRESSIVE WATER WAVES

Omar H. Shemdin

Department of Coastal and Oceanographic Engineering,
University of Florida, Gainesville, Florida

ABSTRACT

An investigation of the air velocity profile above progressive, mechanically-generated waves was made in the wind and wave facility at Stanford University. The influence of propagating waves on the mean velocity profile was sought especially.

Both the instantaneous and mean velocity profiles were obtained with the use of high response total head and static pressure probes, in conjunction with a wave height gage. Experimental evidence is presented which suggests that the air velocity field responds to the wave motion.

The dependence of the mean velocity profile on wave frequency was investigated experimentally over mechanically generated waves having a constant amplitude. Also, the dependence of the mean velocity profile on wave amplitude was investigated over mechanically-generated waves with a specified frequency.

The theoretical results suggest that the wave influence is threefold. The first is due to the fact that a velocity-measuring instrument continuously shifts streamlines when measuring the air velocity above a perturbed water surface. The second is due to the wave-induced perturbation in the air velocity. The third is due to the interaction between the two effects just described. The results contribute towards explaining the lack of consistency in the existing data.

INTRODUCTION

In the study of the aerodynamic drag on the water surface, the method of attack was to relate the properties of the wind to the slope of the mean water level, the surface currents, and the waves generated. The total drag coefficient is usually defined

$$C_n = \frac{D}{\rho U_n^2}, \quad (1)$$

where D is the total drag per unit area at the water surface and U_n is a velocity at height y above the water surface. Keulegan found that C_n increases linearly with U_n in wind channel experiments (ref. 1). Results similar to Keulegan's were found by Fitzgerald in another wind channel and by Van Dorn in a pond (ref. 2 and 3). The increase in the total drag coefficient was also observed by Francis, Sibul, and Hidy and Plate under laboratory conditions, and by Sheppard and Omar in the ocean (ref. 4, 5, 6, and 7). Large scatter in the total drag coefficient was reported by Keulegan and by Johnson and Rice under laboratory conditions, and by Hellström in the field with little evidence that it followed any stress law (ref. 8, 9, and 10). More recently, Kato and Takemura have reported a decrease in the drag coefficient with increasing U_n (ref. 11).

Munk derived an analytical expression for the total drag at the water surface based on the Jeffreys sheltering hypothesis and predicted an increase in the total drag coefficient with increasing U_n (ref. 12). A similar theoretical result was reported recently by Hino (ref. 13). An expression by Neumann, however, predicts a decrease in the total drag coefficient with increasing U_n (ref. 14). Roll, in a review of the studies related to the aerodynamic drag on the water surface, concluded that the state of knowledge is far from satisfactory (ref. 15).

The air velocity profile with respect to the mean water level has been approximated, most commonly, by a logarithmic velocity distribution given by

$$U = \frac{U_*}{\kappa} \ln \frac{y}{z_0} \quad (2)$$

where $U_* = [\tau_0/\rho]^{1/2}$, τ_0 is the surface shearing stress, κ is the Kármán universal constant, z_0 is the roughness height. The uncertainty in determining the mean water level accurately leaves room to adjust the velocity data so that it can be approximated by a logarithmic distribution, whence values of U_* and z_0 are obtained. If the assumption is made that $\tau_0 = D$, then

$$C_n = \left| \kappa / \ln \left(\frac{y_n}{z_0} \right) \right|, \quad (3)$$

which implies that C_n depends on z_0 and the height y_n at which the reference velocity U_n is taken. It is natural to expect that z_0 be related to the characteristics of the propagating waves at the air-water surface. Evidence of such dependence was given by Kunishi for very small amplitude waves (ref. 16). Holmes, however, found no correlation between z_0 and wave characteristics (ref. 17).

The results of previous investigators do not agree on a common relationship between U_* and z_0 as shown in Fig. 1. The disagreement leaves room to question the validity of applying a logarithmic velocity distribution to a shear flow over the water surface. A logarithmic fit was observed by some authors to be reasonable over a portion of the velocity data only. Thus, the

conclusions of Kato and Takemura were based on fitting a logarithmic distribution to the measured velocities close to the water surface, while the conclusions of Francis were based on fitting a logarithmic distribution to the measured velocities away from the water surface (ref. 11 and 18). The aim of the present study is to investigate both experimentally and theoretically the effect of propagating water waves on the measured mean velocity profile in the air stream above the water surface.

EXPERIMENTAL APPARATUS AND PROCEDURE

The 115-foot-long, 74-1/2-inch-high, and 35-1/2 inch-wide wind and wave facility at the Stanford University Hydraulics Laboratory was used for this study. A description of this facility was given by Shemdin and Hsu (ref. 19). The facility wave generator is equipped with an electrohydraulic control system which is capable of generating simple waves ranging in frequency from 0.2 to 4.0 cps. The air intake is located 17 feet downstream of the wave generator plate so that the mechanically generated waves become fully established before exposure to wind. A suction fan is provided at the downstream end of the channel. The fan is driven by a motor capable of creating a maximum wind speed of 80 fps when the water level is at a nominal depth of 3 feet. The channel has a steel plate floor, glass walls in the test section, and is closed by 3-foot by 5-foot interchangeable roof plates. The instruments are mounted on a special 3-foot by 5-foot plate which can be placed at any station along the channel.

The velocity in the air was measured with total head and static-pressure probes, in conjunction with a Pace differential pressure transducer (Model P90D) and a Sanborn 650-1100 series optical-type recorder. Two types of velocity probes were used:

1. a 1/32-inch O.D. pitot-static probe to obtain time-average velocities at a point. The probe is a standard shelf item manufactured by United Sensors and Control Corporation, and has a low cut-off frequency in its response characteristics;
2. a 3/32-inch O.D. total head and static-pressure probe to measure the instantaneous fluctuations of air velocities due to the perturbed water surface. The frequency response was flat up to about 3 cps, which is beyond the frequency range in the present investigation.

The Pace differential pressure transducer was calibrated with a Harrison micromanometer. The effect of both temperature and humidity were taken into account in converting the dynamic head signal into velocity.

The instantaneous velocities above simple mechanically generated waves were obtained by simultaneously recording the dynamic head signal and the water surface elevation. At each fixed position above the mean water level, a recording was obtained. Recordings were obtained at different preselected elevations above the mean water level to adequately describe the instantaneous boundary layer. The water surface elevation was measured by a capacitance-type wave height gage. A Nyclad insulated wire, No. 36 HNC, with

0.006-inch O.D. was used as a sensor. Adequate linearity was obtained in the relationship between the change in the water surface elevation and the voltage change due to wetting the sensor.

The instantaneous velocity at a fixed position above the crest of a mechanically-generated wave was obtained by averaging instantaneous dynamic head values which correspond in time to the wave crest. The crest velocity was typically obtained from an average over ten waves (*i.e.*, an average of ten crest dynamic head values). The position of the velocity probe above the wave crest was obtained from the initial position of the probe above the mean water level and the instantaneous water surface elevation. The crest velocity profile was obtained by simply graphing the crest velocities at different elevations above the mean water level with respect to the wave crest. A velocity profile over the trough was obtained by a similar procedure.

The mean velocity at any elevation above the mean water level was obtained by averaging the dynamic head signal at that level. The mean velocity profile was obtained by graphing the velocity at different elevations above the mean water level with respect to the mean water level. The change in the mean water level due to wind (set-up) was taken into account. The latter was found to be small.

EXPERIMENTAL RESULTS

The influence of surface waves on the mean air velocity profile can be evidenced by comparing: (1) a mean velocity profile over wind-generated waves to (2) one over a rigid flat plate under otherwise identical conditions. The wind-and-wave facility offers a unique possibility for such a comparison since the facility is enclosed by smooth roof plates. At any station the velocity profile vertically upward from the mean water level (profile above water surface) can be compared to the velocity profile vertically downward from the roof (profile over a rigid flat plate). Such a comparison at Station 32.5 (32.5 feet from air intake to test section) is shown in Fig. 2. The intake conditions were shown by Shemdin and Hsu (ref. 19).

Instantaneous velocity profiles were obtained over both the crest and trough of a mechanically-generated wave having a wave height of 3.4 inches and a wave frequency of 0.6 cps. Three trough and three crest profiles were obtained at three different fan speeds at Station 17.5. The instantaneous profiles are shown in Fig. 3. The corresponding mean velocity profiles are shown in Fig. 4. The mean velocity profiles are approximated by logarithmic distributions by the method of least squares.

Further evidence indicating the influence of waves on the mean air velocity profile is given by comparing: (1) the mean velocity profiles over wind-generated waves to (2) those over wind-and-mechanically-generated waves, under otherwise identical conditions. The velocity profiles over wind waves only are shown in Fig. 5 for three fan speeds at Station 57.5. The velocity profiles over wind-and-mechanically-generated waves are shown in Fig. 6 for the same fan speeds and at the same station. The velocity profiles in Figs. 5 and 6 are approximated by logarithmic distributions by the

method of least squares. The logarithmic distribution is seen reasonable for the velocity profiles in Fig. 6 but not for those in Fig. 5.

The influence of the waves on the air velocity profile shown above suggests a more detailed study of the dependence of the air velocity profile on the amplitude and frequency of waves. For this purpose a comprehensive study was made of the mean velocity profile at Station 47.5 so that the geometrical effects of the air entrance and exit of the wind-wave facility can be minimized. Two sets of mean velocity profiles were obtained. The first was over mechanically-generated waves with a constant amplitude and varying frequency. The second was over mechanically-generated waves with a constant frequency and varying amplitude. The frequencies used for the first set were 0.6, 0.75, 1.0, and 1.20 cps. The amplitude used for the first set was 2.00 inches. For each frequency five distinct velocity profiles were obtained at different fan settings with maximum velocity ranging from 13.0 to 40.0 fps.

The frequency used for the second set of velocity profiles was 0.75 cps. The corresponding amplitudes were 1.1, 2.0, and 3.0 inches. For each amplitude, five distinct velocity profiles were obtained at different fan settings with the maximum velocities ranging from 13.0 to 40.0 fps. The velocity profiles of the second set for amplitudes 1.1 and 3.0 inches are shown in Figs. 7 and 8 respectively.

From the velocity profiles of the first set the customary relationship between U_* and z_0 was investigated for each frequency. The results are shown in Fig. 9. The dependence of z_0 on wave frequency was also investigated and the results are shown in Fig. 10. More details on the dependence of U_* and z_0 on both wave amplitude and frequency were given by Shemdin (ref. 20). Previous investigators have attempted to find a relationship between z_0 and U_* as suggested by the data in Fig. 1. A dimensionless graph of gz_0/U_*^2 vs. C/U_* is a convenient artifice to investigate the influence of waves on z_0 and U_* . A dimensionless graph which includes all the acquired data in this study is given in Fig. 11. The graph indicates that C/U_* is an important parameter which influences the relationship between U_* and z_0 . The relationship suggested by Charnock (on purely dimensional grounds) is also shown for comparison (ref. 21).

THEORETICAL ANALYSIS

A standard method for measuring the velocity above a perturbed water surface is to measure the time average dynamic head (*i.e.*, the average difference between the total head and static pressure) at a fixed position of the probe above the mean water level. The measured dynamic head p at any point in the flow field can be expressed

$$p = \frac{\rho}{2} \frac{1}{T} \int_0^T u^2(x, \zeta, t) dt \quad (4)$$

where ζ is the elevation of the probe above the instantaneous water

surface and is consequently a function of time t , u is the air velocity at elevation ζ and station x along the direction of flow, T is the length of time over which the averaging process is considered, and ρ is the air density. The aim of the present analysis is to investigate the variation of p above the mean water level when the water surface is disturbed by a simple, small-amplitude, progressive water wave and the undisturbed mean velocity has a logarithmic profile. The turbulent fluctuation is considered only insofar as they affect the unperturbed mean velocity profile.

The velocity $u(\zeta, t)$ at a station x_0 can be expressed in terms of a mean velocity $U(\zeta)$ and a wave-induced perturbation velocity $u'(\zeta, t)$

$$U(\zeta, t) = U(\zeta) + u'(\zeta, t). \quad (5)$$

The behavior of $u'(\zeta, t)$ was predicted by Miles for a mean velocity profile given by Eq. (2) (ref. 22). Turbulent fluctuations were neglected in the flow field above perturbed water surface. The water surface η was described by

$$\eta = a \exp ik(x - ct), \quad (6)$$

where a is the wave amplitude, k is the wave number, and x is the axis along which the wave propagates with a phase speed c . The real part of η is taken as the actual perturbed surface. The unperturbed mean velocity profile $U(\zeta)$ was described

$$U(\zeta) = U_1 \ln \frac{\zeta}{z_0}, \quad (7)$$

where U_1 is U_s/κ . The flow field considered by Miles has no upper bound, and the perturbation velocity was defined (ref. 22).

$$u'(\zeta, t) = -k\eta U_1 \frac{\partial \phi}{\partial \zeta}, \quad (8)$$

where ϕ is a complex function which satisfies the inviscid Orr-Sommerfeld equation and the surface condition, and decays as $y \rightarrow \infty$. A numerical solution of the boundary value problem governing ϕ was given by Conte and Miles and their results will be used in this investigation to predict the dynamic head above the mean water level (ref. 23).

At an arbitrary station $x = 0$, the position of a probe fixed in space at a specified distance y above the mean water surface, can be expressed in terms of its distance to the instantaneous water surface. The water surface motion is periodic at $x = 0$

$$\eta = a \cos kct, \quad (9)$$

so that

$$\zeta = y - a \cos kct, \quad (10)$$

as shown schematically in Fig. 12.

The dynamic pressure p at any elevation y above the mean water level can be obtained by expressing ζ in terms of y and t in Eq. (4) and integrating with respect to time. The wave-induced perturbation velocity may be expressed at $x = 0$

$$u'(\zeta, t) = kaU_1g(\zeta) \cos(kct - \theta), \quad (11)$$

where

$$g(\zeta) = \left| \frac{\partial \phi(\zeta)}{\partial \zeta} \right|, \quad (12)$$

and

$$\theta = \tan^{-1} \frac{I_m(\partial \phi / \partial \zeta)}{R_e(\partial \phi / \partial \zeta)} + \pi. \quad (13)$$

The dynamic pressure may then be expressed (it is recognized that the angle between the pitot-static probe and the resultant velocity vector is small above small-amplitude waves)

$$p(y) = \frac{\rho}{2} \frac{1}{T} \int_0^T \left| U(y - a \cos kct) + kaU_1g(y-a \cos kct) \cos(kct - \theta) \right|^2 dt, \quad (14)$$

where $g(\zeta)$ and θ are obtained from the numerical solution given by Conte and Miles (ref. 23). The function g is shown typically in Fig. 13 for a wave number k equal to 0.5 ft^{-1} , and an air velocity profile specified by U_1 equal to 3.4 fps and z_0 equal to 0.05 in. Conveniently, the function g may be approximated by an exponential function

$$g(\zeta) = C_1 e^{-h\zeta}, \quad \zeta \leq \zeta_0 \quad (15)$$

and

$$g(\zeta) = C_2, \quad \zeta > \zeta_0 \quad (16)$$

where C_1 , C_2 , and h are constants. The above approximation is also shown graphically in Fig. 13.

The dynamic pressure p , given by Eq. (14), may be expanded into three integrals

$$p(y) = \frac{\rho}{2} (I + II + III). \quad (17)$$

The integral expression I represents the effect of a probe crossing streamlines above a perturbed surface and is given by

$$I = \frac{1}{T} \int_0^T U_1^2 \left| \ln \frac{(y - a \cos kct)}{z_0} \right|^2 dt. \quad (18)$$

The integral expression II represents the interaction effect between crossing streamlines and wave-induced velocity perturbation and is given by

$$II = \frac{2kaU_1^2}{T} \int_0^T \ln \left(\frac{y - a \cos kct}{z_0} \right) g(y - a \cos kct) \cos(kct - \theta) dt. \quad (19)$$

The integral expression III represents the effect of wave-induced perturbation on the velocity measurement and is given by

$$\text{III} = \frac{(kaU_1)^2}{T} \int_0^T g^2(y - a \cos kct) \cos^2(kct - \theta) dt. \quad (20)$$

The logarithmic mean velocity may be expressed in a series to $O[(a/y)^4]$

$$U(\zeta) = U_1 \ln \frac{y}{z_0} - U_1 \left[\left(\frac{a}{y} \right) \cos kct + \frac{1}{2} \left(\frac{a}{y} \right)^2 \cos^2 kct + \frac{1}{3} \left(\frac{a}{y} \right)^3 \cos^3 kct + \frac{1}{4} \left(\frac{a}{y} \right)^4 \cos^4 kct + \dots \right], \quad -1 \leq \frac{a}{y} < 1. \quad (21)$$

The dynamic pressure p in the region $\zeta < \zeta_0$ may be evaluated by substituting Eqs. (15 and 21) into Eq. (14). The dynamic pressure p in the region $\zeta \leq \zeta_0$ becomes for $a < y$ to $O[(a/y)^4]$

$$\begin{aligned} p = \frac{\rho}{2} & \left\{ \left(U_1 \ln \frac{y}{z_0} \right)^2 - \frac{1}{2} [U_1^2 \ln \frac{y}{z_0} - U_1^2] \left(\frac{a}{y} \right)^2 \right. \\ & - \left. \frac{3}{8} \left[\frac{1}{2} U_1^2 \ln \frac{y}{z_0} - \frac{11}{12} U_1^2 \right] \left(\frac{a}{y} \right)^4 \right\} \\ & + \left\{ 2C_1 ka U_1^2 \exp(-2hky) \cos \theta \left[\frac{1}{2} hka \ln \frac{y}{z_0} - \left(\frac{a}{y} \right) \right] \right. \\ & + \left. \frac{3}{8} \left(\frac{hka}{6} \right)^3 \ln \frac{y}{z_0} - \frac{1}{3} \left(\frac{a}{y} \right)^3 - \frac{1}{2} (hka)^2 \left(\frac{a}{y} \right) \right. \\ & - \left. \frac{1}{2} (hka) \left(\frac{a}{y} \right)^2 + \dots \right\} \\ & + \left\{ C_1^2 (ka)^2 U_1^2 \exp(-2hky) \left[\frac{1}{2} + \frac{(hka)^2}{4} (2 + \cos \theta) \right. \right. \\ & \left. \left. + \frac{(hka)^4}{24} (3 + 2 \cos 2\theta) \right] \right\}. \quad (22) \end{aligned}$$

In the region $\zeta > \zeta_0$ the dynamic pressure p becomes for $a < y$ to $O[(a/y)^4]$

$$\begin{aligned} p = \frac{\rho}{2} & \left\{ \left(U_1 \ln \frac{y}{z_0} \right)^2 - \frac{1}{2} [U_1^2 \ln \frac{y}{z_0} - U_1^2] \left(\frac{a}{y} \right)^2 \right. \\ & - \left. \frac{3}{8} \left[\frac{1}{2} U_1^2 \ln \frac{y}{z_0} - \frac{11}{12} U_1^2 \right] \left(\frac{a}{y} \right)^4 + \dots \right\} \end{aligned}$$

$$\begin{aligned}
 & - \left| ka U_1^2 C^2 \left[\left(\frac{a}{y} \right) + \frac{1}{4} \left(\frac{a}{y} \right)^3 + \dots \right] \right| \cos \theta \\
 & + \frac{1}{2} (ka)^2 U_1^2 C^2 \} . \quad (23)
 \end{aligned}$$

The apparent velocity which is extracted from the dynamic pressure is

$$U_{app} = [2p/\rho]^{1/2} . \quad (24)$$

The effects of shifting streamlines and wave-induced perturbation are shown typically in Fig. 14 for the case of an undisturbed logarithmic distribution with U_1 equal to 3.4 fps and z_0 equal to 0.05 inches and a propagating wavy surface with an amplitude of 1.70 inches and a wave number of 0.5 ft^{-1} . It is suggested that the two effects may be compensating. The interaction effect is appreciable, as shown also in Fig. 14.

The above analysis suggests that the measurements of the mean velocity profile above a perturbed water surface depend upon the properties of the propagating waves at the surface. Such an effect has been discounted in the past and thus may constitute the reason for the existing disagreement between the results of previous experimental investigators. The expressions developed for the apparent velocity profile lend themselves readily to numerical evaluation on the computer. The IBM 7090 was used in the present investigation.

DISCUSSION OF RESULTS

The theoretical and experimental results arrived at in this investigation can be viewed as two independent sets of results both aimed at investigating the influence of surface waves on the mean velocity profile above the surface. Conveniently, the theoretical results are discussed first and then the experimental results are explained in light of the theoretical results.

The theoretical results suggest that when a truly logarithmic velocity profile exists over an undisturbed surface, the measurement of such a profile by a pitot-static probe over a surface disturbed by a propagating wave may give a velocity profile which is significantly different from the original profile. The difference between the two profiles is seen to be due to three effects. These are conveniently referred to as the effect of shifting streamlines, the wave-induced perturbation effect, and the interaction between these two effects.

The effect of shifting streamlines is due to the fact that a probe fixed in space above a perturbed surface intercepts different streamlines when the probe is over the wave crest, than when it is over the wave trough. This is shown schematically in Fig. 12. This effect is analogous to that caused by a probe oscillating in a boundary layer above a fixed flat plate. In a turbulent velocity profile, the effect of shifting streamlines gives a velocity which

is less than the true velocity. The effect depends strictly on the shape of the original velocity profile and the ratio of the amplitude of the wave to the height of the probe above the mean water level. The effect is independent of the wave frequency. A numerical computation of this effect is shown in Fig. 14 for the case of an undisturbed logarithmic velocity profile with U_1 equal to 3.4 fps and z_0 equal to 0.05 inch and a propagating wavy surface with an amplitude of 1.7 inches and a wave number of 0.5 ft^{-1} .

The wave-induced perturbation effect is due to the fact that the instantaneous velocity profile over the crest is different from that over the trough of a perturbed water surface as shown in Fig. 3. According to Miles this effect depends on $g(\zeta)$, θ , ka , and U_1 . This effect decays rapidly with increasing distance from the mean water level when compared to the effect of shifting streamlines.

The interaction between the effect of shifting streamlines and the wave-induced effect may either increase or decrease the measured velocity, depending on the coupling between the wave-induced effect and the effect of shifting streamlines. Thus a velocity probe, for example, may gauge a higher velocity over the crest of a wave due to the wave-induced perturbation effect, even though the probe is at a velocity region closer to the boundary.

The predicted influence of wave amplitude on the measured velocity profile is shown in Fig. 15 for the same undisturbed velocity profile and wave frequency discussed above. The wave-induced effect appears to be relatively significant for small-amplitude waves and is consistent with the rapidly decaying property of this effect with height above the perturbed surface. The effect of shifting streamlines becomes dominant for large-amplitude waves. The results of Fig. 15 suggest that high values of both U_1 and z_0 will be measured when compared to the corresponding values of U_1 and z_0 of the undisturbed profile. The overestimate increases with increasing amplitude.

The predicted influence of wave frequency on the measured velocity profile is shown in Fig. 16 for waves having the same amplitude and the same undisturbed velocity profile discussed above. The wave-induced effect decays exponentially upwards from the mean water level. The decay factor depends directly on the wave number k . Consequently, the wave-induced effect in a high-frequency wave (large wave number) is expected to be smaller than that for a relatively lower-frequency wave. The effect of shifting streamlines, however, is independent of the wave frequency as it has already been noted. The interaction effect depends on both wave amplitude and frequency. For the 0.4 and 0.6 cps waves in Fig. 16, the interaction effect is of the same order of magnitude as the effect of shifting streamlines. The interaction effect in these cases is also in the same direction as that due to the shifting of streamlines. The two effects add up to a significant deviation from the undisturbed velocity profile. Contrary to the above, the interaction effect is small compared to the effect of shifting streamlines for the 1.0 and 1.4 cps waves in Fig. 16. The wave-induced effect is also relatively

small, so that most of the deviation indicated is due to the effect of shifting streamlines. The results shown in Fig. 16 suggest that at certain frequencies the velocity profile may deviate significantly from a velocity profile over an undisturbed water surface.

In conclusion it is emphasized that the present theoretical analysis is valid only insofar as the water surface is perturbed by a simple propagating wave, and only insofar as the Miles inviscid Reynolds stress mechanism remains valid. Recent work by Bryant suggests that the inviscid Reynolds stress mechanism underestimates the transfer of energy to waves (ref. 24). No analytic solution of the wind field was proposed, however, to replace Miles's solution. The present theoretical analysis can be extended to any wind flow field if it can be described analytically. Within the above restrictions the results of Figs. 15 and 16 suggest, as a rule of thumb, that the influence of waves on the measured velocity profile becomes small at an approximate distance of three amplitudes above the mean water level.

It is to be noted again that the theoretical predictions shown in Figs. 15 and 16 are for an undisturbed logarithmic profile which corresponds to a fan speed of 240 rpm. At different fan speeds, the theoretically predicted wave-influenced velocity profiles are expected to be different. The different behaviors indicated in Figs. 10 and 11 for different wind speeds may be explained in light of the two competing influences and their interaction, all of which are induced by the presence of waves.

The present investigation in no way gives an answer to the question of whether the actual velocity profile over a disturbed surface is truly logarithmic. It only suggests that if it is logarithmic, then the measured profile by a velocity probe would deviate from the true velocity profile. The fact that the velocity profiles over wind-generated waves, shown in Fig. 5, deviate from a logarithmic distribution still remains to be explained. The theoretical results presented in this investigation predict a deviation from the logarithmic distribution in the opposite direction from that shown in Fig. 5. The fact that the measured velocity profiles over mechanically-generated waves shown in Fig. 6 come closer to the logarithmic distribution, is consistent with the theoretical results of this investigation. Stewart suggested that the velocity profile over a wavy surface may deviate from a logarithmic distribution in a manner similar to the profiles shown in Fig. 5 (ref. 25). More recently, however, Phillips has discounted such a behavior (ref. 26).

REFERENCES

1. Keulegan, G. H. Wind Tides in Small Closed Channels, 1951, *J. Res. Natl. Bureau of Standards*, **46**, 258-381.
2. Fitzgerald, L. M. Wind-Induced Stresses on Water Surfaces: A Wind Tunnel Study, 1963, *Austr. J. Phys.*, **16**, 475-489.

3. Van Dorn, W. G. Wind Stress on an Artificial Pond, 1953, *J. Mar. Res.*, **12**, 249-276.
4. Francis, J. R. D. Wind Stresses on a Water Surface, 1954, *Quart. J. Roy. Met. Soc.*, **80**, 438-443.
5. Sibul, O. Laboratory Study of the Generation of Wind Waves in Shallow Water, 1955, *Beach Erosion Board T. M.* 72, Washington.
6. Hidy, G., and Plate, E. Wind Action on Water Standing in a Laboratory Channel, 1966, *J. Fluid Mech.*, **26**, 651-687.
7. Sheppard, P. A., and Omar, M. H. The Wind Stresses over the Ocean from Observations in the Trades, 1952, *Quart. J. Roy. Met. Soc.*, **78**, 583-589.
8. Keulegan, G. H. Hydrodynamic Effects of Gales on Lake Erie, 1953, *J. Res. Natl. Bureau of Standards*, **50**, 99-109.
9. Johnson, J. W., and Rice, E. K. A Laboratory Investigation of Wind Generated Waves, 1952, *Trans. A. G. U.*, **33**, 845-854.
10. Hellström, B. Wind Effect on Rinköbing Fjord, 1953, *Trans. A. B. U.*, **34**, 194-198.
11. Kato, H., and Takemura, K. Wind Profiles over the Shallow Water (1st Report), 1966, *Port and Harbor Tech. Res. Inst.*, **5**, No. 1.
12. Munk, W. H. Wind Stresses on Water: A Hypothesis, 1955, *Quart. J. Roy. Met. Soc.*, **81**, 320-332.
13. Hino, M. A Theory on the Fetch Graph, the Roughness of the Sea and the Energy Transfer between Wind and Wave, 1966, *Proc. 10th Conf. Coastal Engrg.*, **1**, Tokyo, 18-30.
14. Neumann, G. Über den Tangential druck des Windes und die Ranigkeit der Meeresoberfläche, 1948, *Z. Met.*, **2**, 193.
15. Roll, H. U. On the Present State of Knowledge in Air-Sea Boundary Layer Problems, 1965, *Proc. Sea-Air Interaction Conf.* (Tallahassee, Florida, Feb., 1965), Tech. Note 9-SAIL, ESSA, Washington 30-58.
16. Kunishi, H. An Experimental Study on the Generation and Growth of Wind Waves, 1963, *Diss. Prev. Res. Inst.*, Bull. **61**, Kyoto.
17. Holmes, P. Wind Generation by Waves, 1963, Ph.D. Thesis, College of Swansea, Univ. of Wales.

18. Francis, J. R. D. The Aerodynamic Drag of a Free Water Surface, 1951, *Proc. Roy. Soc.*, Ser. A, 206, 387-408.
19. Shemdin, O. H., and Hsu, E. Y. The Dynamics of Wind in the Vicinity of Progressive Water Waves, 1966, *Proc. 10th Conf. on Coastal Engineering*, Tokyo, 396-317.
20. Shemdin, O. H. Experimental and Analytical Investigation of the Air Velocity Profile Above Progressive Waves, 1967, *Dept. of Civil Eng. Tech. Rept.*, 82, Stanford Univ., Stanford.
21. Charnock, H. Wind-Stress on a Water Surface, 1955, *Quart. J. Roy. Met. Soc.*, 81, 639.
22. Miles, J. W. On the Generation of Surface Waves by Shear Flows, 1957, *J. Fluid Mech.*, 3, 185-204.
23. Conte, S. D., and Miles, J. W. On the Numerical Integration of the Orr-Sommerfeld Equation, 1959, *J. Soc. Indust. Appl. Math.*, 7, 361-366.
24. Bryant, P. J. Wind Generation of Water Waves, 1966, Ph.D. Dissertation, Univ. of Cambridge.
25. Stewart, R. W. The Drag of Wind over Water, 1961, *J. Fluid Mech.*, 10, 189-194.
26. Phillips, O. M. The Dynamics of the Upper Ocean, 1966, Cambridge Univ. Press.

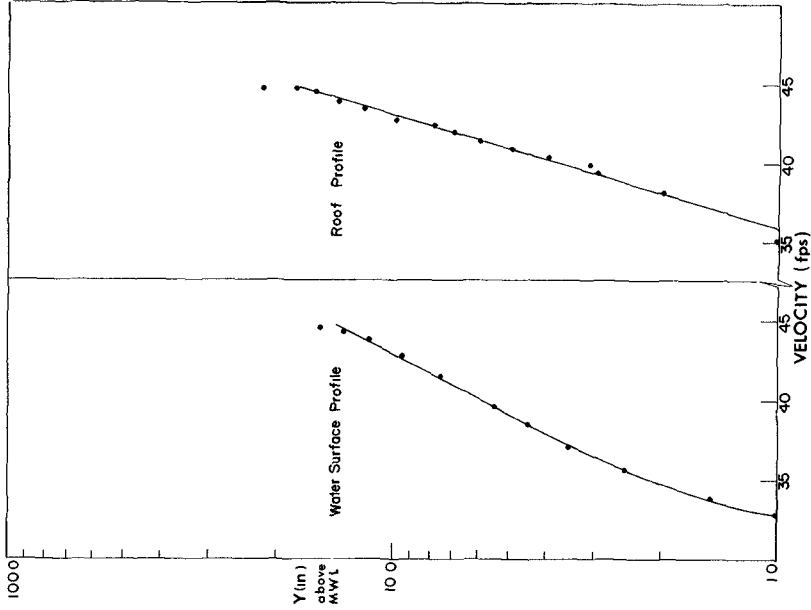


Fig. 2. Comparison between the water surface and flat plate velocity profiles, at Sta. 32.5.

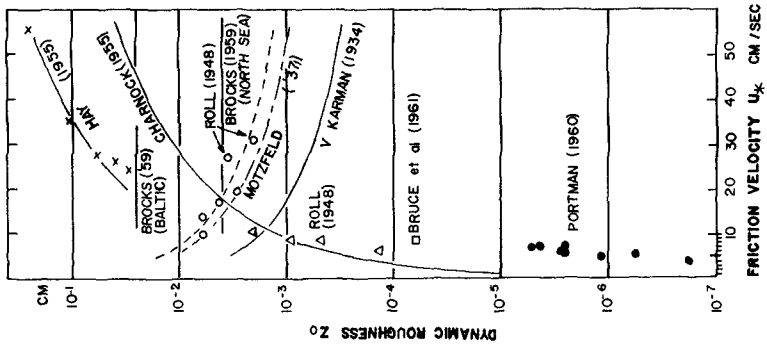


Fig. 1. U_* vs. z_0 after Roll (1965).

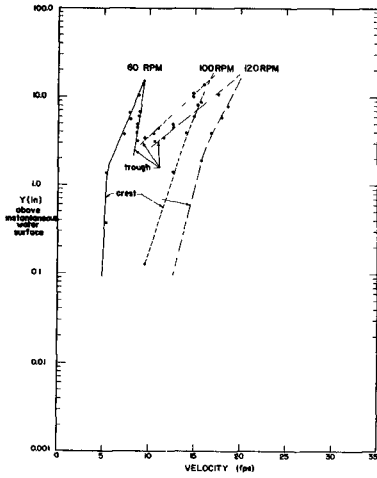


Fig. 3. Instantaneous crest and trough profiles over a mechanically generated wave ($a=1.7$ in., $f=0.6$ cps).

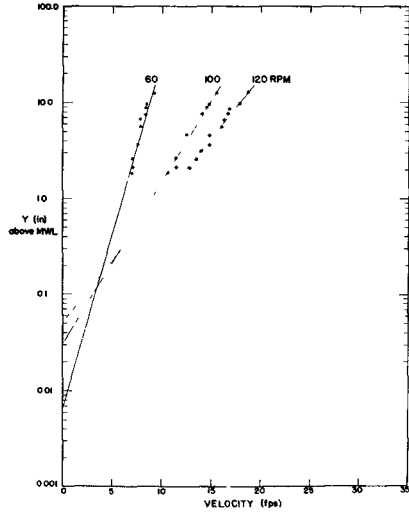


Fig. 4. Mean profiles over a mechanically generated wave ($a=1.7$ in., $f=0.6$ cps).

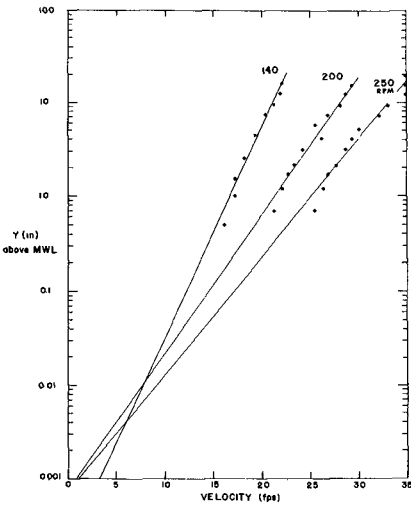


Fig. 5. Mean profiles over water surface perturbed by wind waves only.

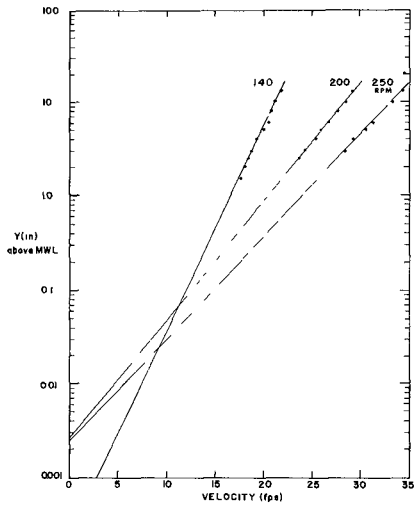


Fig. 6. Mean velocity profiles over water surface perturbed by wind and mechanical waves.

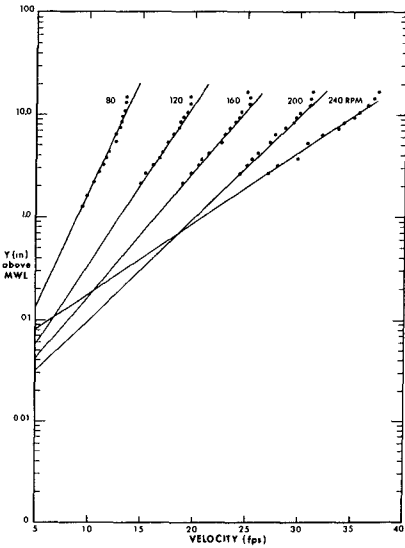


Fig. 7. Mean profiles over a mechanically generated wave ($a=1.10$ in., $f=0.75$ cps).

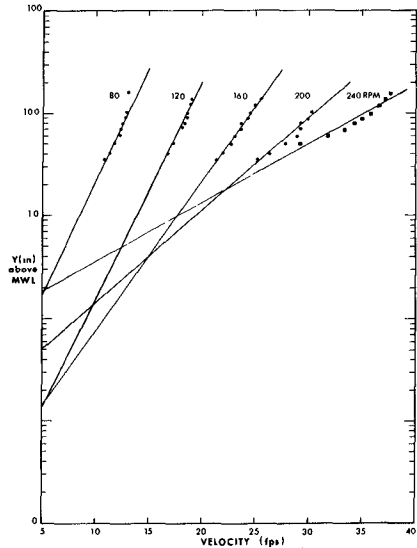


Fig. 8. Mean profiles over a mechanically generated wave ($a=3.00$ in., $f=0.75$ cps).

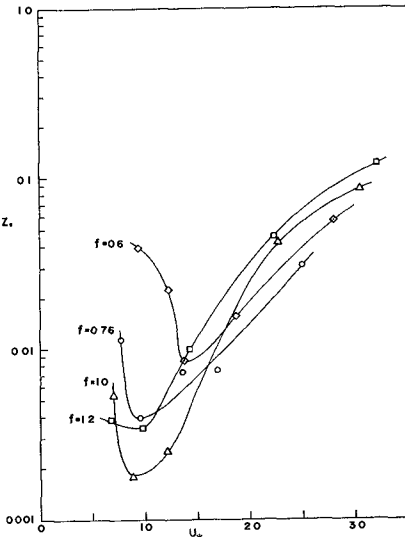


Fig. 9. z_0 vs. U_* at pre-selected frequencies ($a=2.00$ in.).

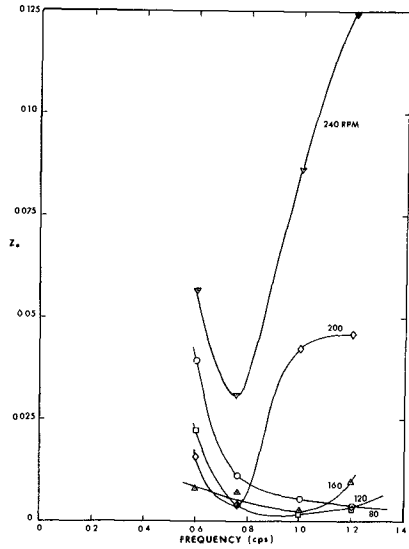


Fig. 10. z_0 vs. f for mechanically generated waves ($a=2.00$ in.).

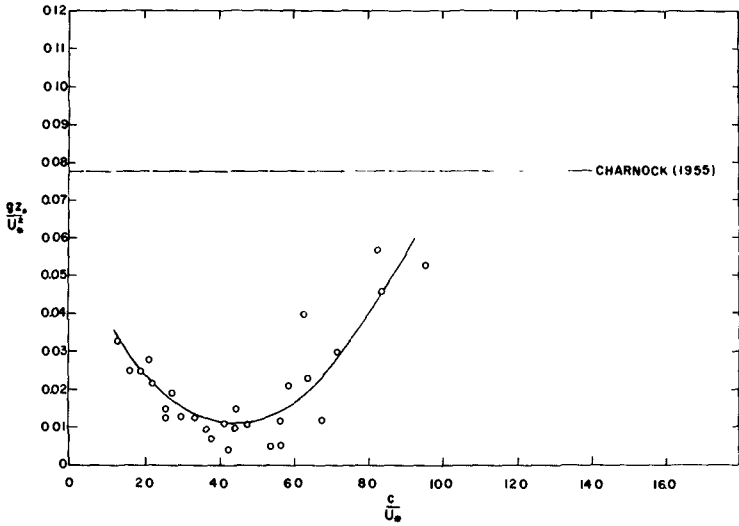


Fig. 11. Dimensionless relationship of all acquired data.

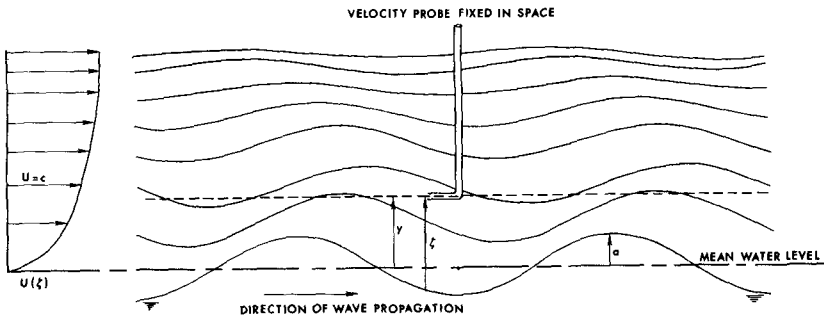


Fig. 12. Schematic diagram of streamlines over a perturbed surface.

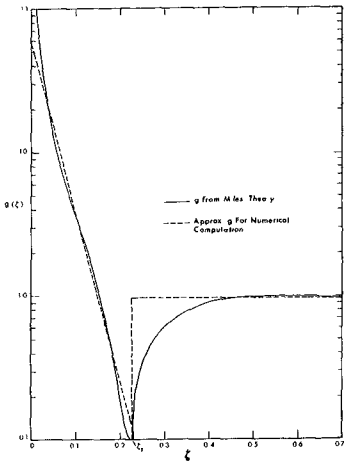


Fig. 13. $g(\zeta)$ vs. $k\zeta$ from Conte and Miles (1959).

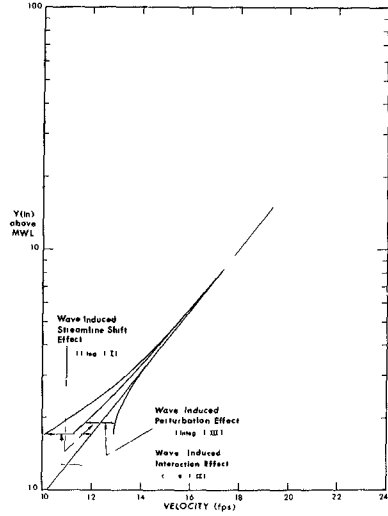


Fig. 14. Theoretically predicted effects of shifting streamlines, velocity perturbation, and interaction of two effects.

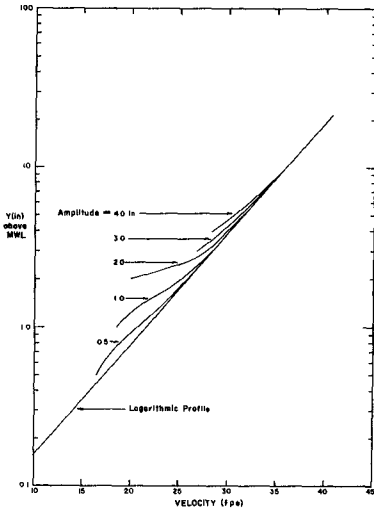


Fig. 15. Predicted wave-influenced mean profiles at different wave amplitudes ($f=0.75$ cps).

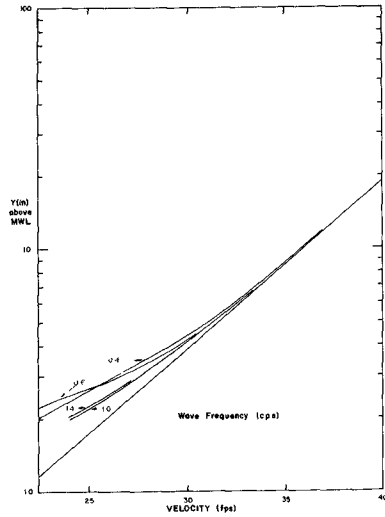


Fig. 16. Predicted wave-influenced mean profiles at different wave frequencies ($a=2.00$ in.).